Acta Biomaterialia 8 (2012) 2483–2492

Contents lists available at SciVerse ScienceDirect

Acta Biomaterialia

journal homepage: www.elsevier.com/locate/actabiomat

Development of silk-based scaffolds for tissue engineering of bone from human adipose-derived stem cells

Cristina Correia [a,b,c], Sarindr Bhumiratana [a], Le-Ping Yan [b,c], Ana L. Oliveira [b,c], Jeffrey M. Gimble [d], Danielle Rockwood [e], David L. Kaplan [e], Rui A. Sousa [b,c], Rui L. Reis [b,c], Gordana Vunjak-Novakovic [a,*]

[a] Laboratory for Stem Cells and Tissue Engineering, Department of Biomedical Engineering, Columbia University, 622 W168th St., Vanderbilt Clinic 12-234, NY 10032, USA
[b] 3B's Research Group – Biomaterials, Biodegradables and Biomimetics, University of Minho, Headquarters of the European Institute of Excellence on Tissue Engineering and Regenerative Medicine, Guimarães, Portugal
[c] ICVS/3B's – PT Government Associate Laboratory, Braga/Guimarães, Portugal
[d] Pennington Biomedical Research Center, Louisiana State University System, Baton Rouge, LA, USA
[e] Department of Biomedical Engineering, Tufts University, 4 Colby Street, Medford, MA, USA

ARTICLE INFO

Article history:
Received 21 November 2011
Received in revised form 8 February 2012
Accepted 7 March 2012
Available online 13 March 2012

Keywords:
Bone
Tissue engineering
Silk
Scaffold
Adipose stem cells

ABSTRACT

Silk fibroin is a potent alternative to other biodegradable biopolymers for bone tissue engineering (TE), because of its tunable architecture and mechanical properties, and its demonstrated ability to support bone formation both in vitro and in vivo. In this study, we investigated a range of silk scaffolds for bone TE using human adipose-derived stem cells (hASCs), an attractive cell source for engineering autologous bone grafts. Our goal was to understand the effects of scaffold architecture and biomechanics and use this information to optimize silk scaffolds for bone TE applications. Silk scaffolds were fabricated using different solvents (aqueous vs. hexafluoro-2-propanol (HFIP)), pore sizes (250–500 μm vs. 500–1000 μm) and structures (lamellar vs. spherical pores). Four types of silk scaffolds combining the properties of interest were systematically compared with respect to bone tissue outcomes, with decellularized trabecular bone (DCB) included as a "gold standard". The scaffolds were seeded with hASCs and cultured for 7 weeks in osteogenic medium. Bone formation was evaluated by cell proliferation and differentiation, matrix production, calcification and mechanical properties. We observed that 400–600 μm porous HFIP-derived silk fibroin scaffold demonstrated the best bone tissue formation outcomes, as evidenced by increased bone protein production (osteopontin, collagen type I, bone sialoprotein), enhanced calcium deposition and total bone volume. On a direct comparison basis, alkaline phosphatase activity (AP) at week 2 and new calcium deposition at week 7 were comparable to the cells cultured in DCB. Yet, among the aqueous-based structures, the lamellar architecture induced increased AP activity and demonstrated higher equilibrium modulus than the spherical-pore scaffolds. Based on the collected data, we propose a conceptual model describing the effects of silk scaffold design on bone tissue formation.

1. Introduction

Numerous approaches have been made towards development of an "ideal" scaffold for bone tissue engineering [1,2]. Silk fibroin, obtained from silkworms, demonstrates great biocompatibility along with outstanding mechanical properties [3] and proteolytic degradation [4]. In tissue engineering, silk fibroin has been extensively used for multiple types of scaffolds [5–8]. Various modifications of silk scaffolds have been fabricated with a wide range of chemical, structural and biomechanical modifications [6,9,10]. Silk sponges have been used for cartilage [11–13] and fat [14,15], silk tubes for blood vessels [16] and silk fibers for ligaments [17,18]. Porous sponge scaffolds are suitable for bone tissue formation, as they enhance cell attachment, proliferation and migration. In addition, the high porosity (92–98%) [19–21] facilitates nutrient and waste transport into and out of the scaffolds.

Porous silk sponges can be fabricated using porogens, gas foaming or lyophilization methods [22,23]. Among these, NaCl salt leaching is one of the simplest and most effective fabrication methods, resulting in scaffolds with spherical pores and different morphologies. Silk scaffolds are generally fabricated using two different silk preparation methods: aqueous and solvent (hexafluoro-2-propanol; HFIP) based. HFIP does not solubilize salt particles, therefore pore sizes in these sponges reflect the size of the porogen used in the process [22,23]. On the other hand, aqueous-based silk sponges demonstrate pore sizes 10–20% smaller than the size of salt crystals. This is due to partial solubilization of the

* Corresponding author. Tel.: +1 212 305 2304.
E-mail address: gv2131@columbia.edu (G. Vunjak-Novakovic).

1742-7061/$ - see front matter © 2012 Acta Materialia Inc. Published by Elsevier Ltd. All rights reserved.
http://dx.doi.org/10.1016/j.actbio.2012.03.019

surface of the salt particles during supersaturation of the silk solution before solidification [3,24]. This partial solubilization results in rougher surfaces of the pores, which improved cell attachment [22,25]. For comparison, aqueous-based processing results in sponges with higher porosity [22,25] and higher degradation rates [22,25].

Besides silk sponges with spherical pores, our laboratory developed a novel silk scaffold fabrication method to produce lamellar-like structure using a freeze drying technique [26]. This structure mimics bone lamellae structure. Human bone marrow mesenchymal stem cells, cultured on osteogenic medium, attached, proliferated and assembled new extracellular matrix on this patterned structure [26].

Tissue engineers have explored silk scaffolds for bone regeneration by using bone marrow mesenchymal stem cells (BM-MSC) as the preferred cell source with superior outcomes validated with both aqueous-based [19,26,27] and HFIP-derived scaffolds [6,21,28]. Human adipose-derived stromal/stem cells (hASCs), on the other hand, present features comparable to BM-MSC and are a promising alternative for cell-based therapies [29] such as bone tissue regeneration. hASCs may be easily isolated from adipose tissue, with a high yield of cells per unit tissue volume [30]. Furthermore, hASCs proliferate quickly, and their osteogenic potential is comparable to that of bone marrow mesenchymal stem cells [31]. Our research group has engineered half-centimeter-sized bone constructs in vitro by using hASCs that were seeded in decellularized bone scaffolds and cultured dynamically in perfusion bioreactors [32].

Silk scaffold and hASCs are two potential components for bone tissue engineering applications, which have not been yet investigated in combination. In this study, five different scaffolds were investigated: (i) aqueous, spherical-pore structure, small pores (250–500 μm); (ii) aqueous, spherical-pore structure, large pores (500–1000 μm); (iii) aqueous, lamellar structure; (iv) HFIP, medium pore sizes (400–600 μm); and (v) decellularized bovine trabecular bone, used as a "gold standard", to evaluate the osteogenic responses of hASCs and bone tissue development.

2. Materials and methods

2.1. Preparation of silk fibroin scaffolds

All chemicals were purchased from Sigma–Aldrich (St. Louis, MO) unless otherwise stated. Silk scaffolds were prepared according to Fig. 1. Silk fibroin from silkworm (*Bombix mori*) cocoons was extracted with 0.02 M sodium carbonate (Na_2CO_3) solution, rinsed in distilled water, dissolved in a 9.3 M lithium bromide (LiBr) solution and dialyzed for 48 h against distilled water in benzoylated dialysis tubing (Sigma D7884). Dissolved silk fibroin was centrifuged for 20 min at 8600*g* (4 °C). The resulting solution was determined by weighing the remaining solid after drying, yielding a 6 wt.% aqueous silk fibroin solution.

Aqueous-derived silk fibroin porous sponges were prepared by salt leaching methods. NaCl salt was sieved with metal mesh to obtain particle size distributions between 250 and 500 μm (Aq-250) or between 500 and 1000 μm (Aq-500), and added into silk fibroin aqueous solution at a 2:1 (w/v) ratio, in disk-shaped containers. The container was covered and left at room temperature. After 24 h, the container was immersed in water to extract NaCl salt for 2 days, with 5–6 water changes per day.

Aqueous-derived silk fibroin lamellar scaffolds (Aq-Lam) were prepared by pouring silk fibroin aqueous solution into silicon tubing (6 mm i.d.), frozen at −80 °C, lyophilized for 1 day, then autoclaved to induce the formation of a β-sheet structure and insolubility in aqueous solution.

HFIP-derived silk fibroin scaffolds (HFIP-400) were prepared as previously described [25]. Silk fibroin aqueous solution was lyophilized and further dissolved with HFIP, resulting in a 17 wt.% HFIP-derived silk fibroin solution. Granular NaCl particles (400–600 μm) were added to 2 ml of silk fibroin in HFIP at 2:1 (w/v) ratio. The containers were covered overnight to reduce evaporation of HFIP and to provide sufficient time for homogeneous distribution of the solution. Subsequently, the solvent was evaporated at room temperature for 3 days. The matrices were then treated in 90 vol.% methanol for 30 min, to induce the formation of the β-sheet structure, followed by immersion in water for 2 days to remove NaCl porogens. Porous silk scaffolds were then freeze-dried. All scaffolds were cut and cored into cylinders of 4 mm diameter and 2 mm thickness.

2.2. Preparation of trabecular bone scaffolds

Trabecular bone scaffolds were decellularized as in our previous studies [32,33]. Trabecular bone cylinders (4 mm diameter) were cored from the subchondral region of carpometacarpal joints of bovine calves and washed with a high-velocity stream of water to remove bone marrow from pore spaces. Scaffolds were further washed for 1 h in phosphate-buffered saline (PBS) with 0.1% ethylenediamine tetraacetic acid (EDTA) at room temperature (RT), followed by sequential washes in hypotonic buffer (10 mM Tris and 0.1% EDTA) overnight at 4 °C, in detergent (10 mM Tris and 0.5% sodium dodecyl sulfate) for 24 h at RT and in enzyme solution (100 U ml^{-1} DNAse, 1 U ml^{-1} RNAse and 10 mM Tris) for 6 h at 37 °C, to fully remove cellular material. Scaffolds were then rinsed in PBS, freeze-dried and cut into 2 mm thick cylindrical plugs. The scaffolds within the density range of 0.28–0.38 mg mm^{-3} (calculated based on the dry weights and exact dimensions) were selected for experiments.

2.3. Isolation, characterization and expansion of hASCs

hASCs were isolated according to previously described methods [34] from liposuction aspirates obtained from the Pennington Biomedical Research Center, under protocols approved by the Institutional Review Board. hASCs were expanded to the fourth passage in expansion medium: high-glucose Dulbecco's modified Eagle's medium (DMEM) supplemented with 10% fetal bovine serum (FBS), penicillin–streptomycin (1%), and 1 ng ml^{-1} basic fibroblast growth factor.

Passage zero (P0) cells were examined for surface marker expression using flow cytometry. The presence of specific antigens such as CD29, CD105, CD45, CD34, CD44, CD73 and CD90 were analyzed, as previously published [34,35]. hASCs were confirmed for their differentiation capacity into the adipogenic and osteogenic lineages in monolayer cultures following induction with adipogenic and osteogenic inductive medium for up to 14 days and histochemical analysis of neutral lipid (Oil Red O) or mineralization (Alizarin Red) staining as published [36].

Three independent series of experiments were performed, each with triplicates of samples for each experimental group, data point and analytical method.

2.4. Construct seeding and culture

All scaffolds were sterilized in 70% ethanol overnight, washed in PBS and incubated in expansion medium 24 h prior to seeding. For construct seeding, expanded P4 hASCs were suspended in culture medium at 3×10^7 cells ml^{-1}. Scaffolds were blot-dried, placed individually into wells of a nontreated 12-well cell culture plate and a 20 μl aliquot of cell suspension was pipetted into each scaffold, and pipetted up and down to ensure even distribution of cells.

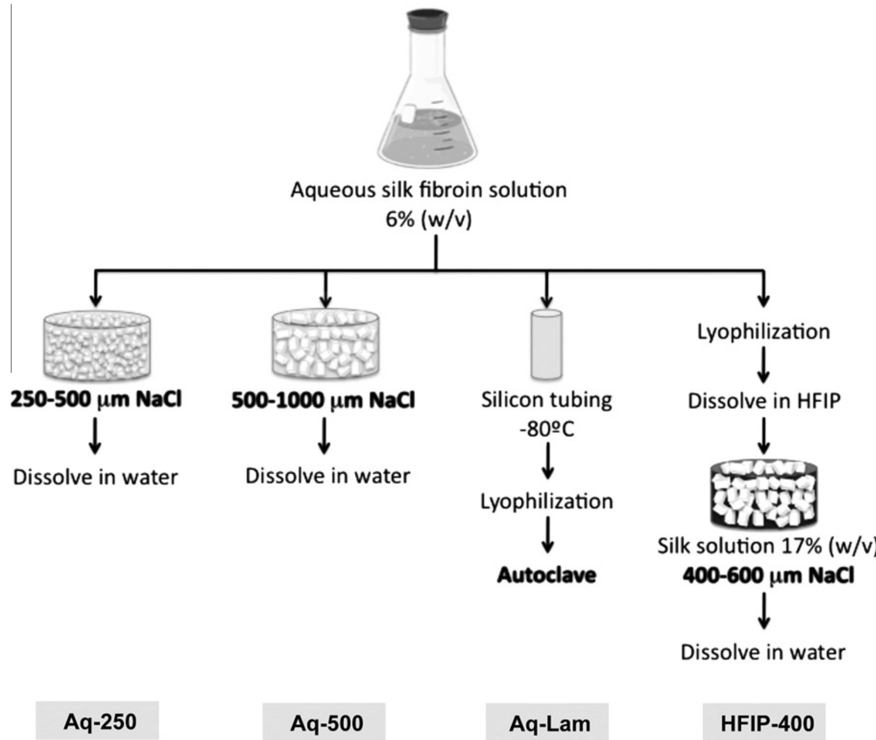

Fig. 1. Silk scaffold fabrication. Silk fibroin is extracted from silkworm cocoons into an aqueous solution. Aqueous-based spherical-pore scaffolds (Aq-250 and Aq-500) are produced by the salt-leaching method, where small (250–500 μm) or large (500–1000 μm) NaCl particles are used as the porogen. Aqueous-based lamellar scaffolds (Aq-Lam) are produced by lyophilizing the frozen aqueous silk solution cast in a silicon tube. HFIP-derived porous scaffolds (HFIP-400) are developed by dissolving the lyophilized aqueous silk solution in HFIP solvent, to which NaCl particles (400–600 μm) are added to form the porous structure. The NaCl particles used in the salt-leaching method are further dissolved in water. Bold text represents the step where β-sheet formation occurs.

After 15 min in the incubator, scaffolds were rotated 180° and 10 μl of cell-free medium was added to maintain hydration. This process was repeated four times to achieve uniform cell distribution, after which osteogenic medium (low-glucose DMEM, 10% FBS, 1% penicillin–streptomycin, 10 mM sodium-b-glycerophosphate, 10 mM HEPES, 100 nM dexamethasone and 50 μg ml^{-1} ascorbic acid-2-phosphate) was added. hASC-seeded scaffolds were maintained in static culture (nontreated 12-well cell culture plate) and nourished with 3 ml of osteogenic medium per well for 7 weeks to induce osteogenic differentiation of the stem cells and to ensure robust bone tissue development.

2.5. Live/Dead assay

A Live/Dead Viability/Cytotoxicity Kit (Molecular Probes, OR, USA) was used to evaluate cell viability. Live cells (indicated by calcein AM) and dead cells (indicated by ethidium homodimer-1) were observed and imaged through a confocal microscope (Leica, Germany). Optical surfaces were taken from the surface to 160 μm deep, at 10 μm intervals. All images are presented as vertical projections.

2.6. Biochemical characterization

Constructs were harvested, washed in PBS, cut in half and weighed. For DNA assay, half of the constructs were added to 1 ml of digestion buffer (10 mM Tris, 1 mM EDTA, 0.1% Triton X-100, 0.1 mg ml^{-1} proteinase K) and incubated overnight at 56 °C for digestion. After centrifugation at 3000g for 10 min, the supernatants were removed, diluted and pippeted in duplicate into a 96-well plate. Picogreen solution (Quant-iT™ PicoGreen® dsDNA Kit, Invitrogen) was added to the samples in 1:1 ratio (v/v). Sample fluorescence was measured with a fluorescent plate reader at an excitation of ~480 nm and an emission of ~520 nm. Lambda DNA was used to prepare the standard curve. Based on previous studies [32], 5 pg of DNA per cell was used as the conversion factor to determine the cell number. For calcium quantification, half of the constructs were incubated in 1 ml of 5 vol.% trichloroacetic acid and calcium was extracted by disintegrating the construct using steel balls and a MinibeadBeater™ (Biospec, Bartlesville, OK, USA). The calcium content and standard were quantified using StanbioTotal Calcium Liquicolor® (Stanbio Laboratory, USA). The sample's optical density was measured at 575 nm using a microplate reader. Alkaline phosphatase (AP) activity was determined by adding cell lysis solution to half of each scaffold, which were then disintegrated using steel balls and a MinibeadBeater™. After centrifugation, 50 μl of supernatant was incubated with 50 μl of *p*-nitrophenyl-phosphate (*p*NPP) substrate solution at 37 °C for 20 min. The reaction was stopped with 50 μl of stop solution, and the absorbance was read at 405 nm. *p*-Nitrophenol at known concentrations was used to prepare the standard curve. All solutions were components of the SensoLyte® *p*NPP Alkaline Phosphatase Complete Kit (Cell Biolabs, CBA-302).

2.7. Histology and immunohistochemistry

After harvest, the samples were fixed in 4% formaldyhyde solution for 1 day. Bone scaffolds were decalcified with immunocal solution (Decal Chemical, Tallman, NY) for 1 day and further dehydrated with graded ethanol washes, concurrently with the rremaining silk constructs. Samples were embedded in paraffin, sectioned in 5 μm slices and mounted on glass slides. For staining, sections were deparaffinized with CitriSolv and rehydrated with a graded series of ethanol washes. Samples were stained using standard hematoxylin and eosin (H&E) staining. Immunohistochemistry was performed on sections as follows: sections were blocked with normal horse serum (NHS), stained sequentially with primary antibody (rabbit anti-human osteopontin (OPN) polyclonal antibody, Chemicon ab1870; rabbit anti-bone sialoprotein (BSP) polyclonal antibody, Millipore ab1854; mouse monoclonal anti-collagen I, Abcam ab6308; NHS for negative control) and secondary antibody (Vectastain Universal Elite ABC Kit, PK-6200 Vector Laboratories), and developed with a biotin–avidin system (DAB Substrate Kit SK-4100, Vector Laboratories).

2.8. Microcomputed tomography (μCT) analysis

Before culture, the architecture of the silk scaffolds was evaluated using a micro-CT Skyscan 1072 scanner (Skyscan, Kontich, Belgium). The X-ray scans were acquired in high-resolution mode with a pixel size of 8 μm, an integration time of 1.3 s, and penetrative X-rays of 35 keV and 209 μA. Data sets were reconstructed using standardized cone–beam reconstruction software (NRecon v1.4.3, SkyScan). A representative data set of the slices was segmented into binary images with a dynamic threshold of 40–255 (grey values), which were used for morphometric analysis (CT Analyser, v1.5.1.5, SkyScan) and to build three-dimensional (3-D) models (ANT 3D creator, v2.4, SkyScan).

After culture, μCT was performed using the protocol described by Liu et al. [37]. Samples were aligned in a 2 ml screw-cap centrifuge tube, which was clamped in the specimen holder of a vivaCT40 system (SCANCO Medical AG, Basserdorf, Switzerland). The 2 mm length of the scaffold was scanned at 21 μm isotropic resolution. A global thresholding technique, which only detects mineralized tissue, was applied to obtain the bone volume (BV) of the samples.

2.9. Scanning electron microscopy (SEM)

Samples were washed in PBS and then fixed in 2% glutaraldehyde in sodium cacodylate buffer for 2 h. Constructs were washed in buffer and freeze-dried overnight. The samples were coated with gold and palladium and imaged in machine scanning electron microscope (JEOL, Japan).

2.10. Mechanical testing

Young's modulus upon compression of constructs after culture was determined under unconfined compression in wet conditions using a modification of an established protocol [38]. An initial tare load of 0.2 N was applied and was followed by a stress–relaxation step, where specimens were compressed at a ramp velocity of 1% s^{-1} up to 10% strain and maintained in that position for 1800 s. The Young's modulus was obtained from the equilibrium forces measured at 10% strain.

2.11. Statistical analysis

Data are presented as mean (three independent series of experiments, each with $n = 3$ per group, data point and analytical assay) ± standard deviation. Statistical significance was determined using analysis of variance followed by Tukey's HSD (honestly significant difference) test using Prism software (Prism 4.0c, GraphPad Software Inc.).

3. Results

3.1. Characterization of undifferentiated hASCs

The immunophenotype of undifferentiated hASCs was evaluated using flow cytometry (Fig. 2A). The antigen expression profile observed was consistent with our previous study [39]: expression of the adhesion molecules integrin β1 (CD29) and endoglin (CD105), high expression of ecto 5′-nucleotidase (CD73) surface enzyme as well as extracellular matrix proteins such as Thy-1 (CD90) and glycoprotein CD34. Hyaluronate (CD44) receptor molecule was expressed to a lesser degree than expected; however, expression of hematopoietic marker CD45 was accordingly very low. Multilineage potential of hASCs was evaluated by cultivation of cell monolayers in adipogenic or osteogenic medium. The isolated hASCs exhibited multi-lineage differentiation, as shown with the formation of Oil Red O staining lipid droplets (Fig. 2C) and Alizarin Red staining extracellular mineralization (Fig. 2D).

3.2. Characterization of silk fibroin scaffolds

The architecture of the aqueous-based silk fibroin scaffolds was characterized by SEM and μCT analysis (Fig. 3). Both SEM imaging (Fig. 3, top) and μCT 3-D reconstructions (Fig. 3, middle) demonstrate the pore morphology of the developed structures. Spherical interconnected pores, forming a trabecular-like network, are observed in the Aq-250 and Aq-500 groups, fabricated by the salt-leaching method with two ranges of porogen size (250–500 and 500–1000 μm, respectively). On the other hand, Aq-Lam presents a structure where the pore walls do not form a sphere, but form parallel lamellae, which are aligned in several directions within the 3-D structure.

Porosity, interconnectivity, pore size and trabeculae thickness were obtained by μCT analysis (Fig. 3, bottom): the Aq-500 structure presents the highest porosity value (86.62 ± 0.84%) and highest average pore size (254.32 ± 13.64 μm), which is explained by the use of bigger NaCl particles. The highest percentage of interconnectivity (97.83 ± 0.61%) was also measured for this group. Characterization of the Aq-Lam demonstrated a more compact structure, with lower porosity (64.25 ± 8.82%) and smaller pore size (126.24 ± 48.16%), and 35% less pore interconnectivity (63.25 ± 21.13%) than Aq-500.

3.3. Cell viability and proliferation

Cell seeding efficiency, calculated as a fraction of the initial cells detected in the scaffold after seeding, ranged from 60% to 75% in all five groups, without statistically significant differences (Fig. 4A). DNA assay (Fig. 4B) demonstrated that, after 2 weeks of culture, proliferation occurred to the same extent (an approximately 1.6-fold increase in cell numbers) in all spherical porous silk sponges, whether aqueous or HFIP based (Aq-250, Aq-500, HFIP-400). In contrast, the lamellar structure maintained the initial cell numbers throughout the culture period. In aqueous scaffolds, the cell numbers achieved by week 2 were maintained through week 7. In the HFIP scaffold group, the cell number increased continuously. In the decellularized bone group, the cell number decreased at the end of the culture period. The Live/Dead assay confirmed the cell viability and attachment throughout all the scaffolds (Fig. 4C).

Good distribution of cells at the periphery and center of the constructs was observed through H&E staining in all groups (Fig. 5 top). Cells attached to scaffold surfaces, and filled the pore spaces. Rough pore surfaces were observed by H&E staining (Fig. 5 top) and SEM (Fig. 5 middle and bottom) in aqueous spherical-pore scaffolds, in contrast to smooth pore surfaces in HFIP scaffolds. The matrix density appeared to be greater in the aqueous porous scaffolds (Aq-250 and Aq-500) and the trabecular bone scaffold than in the HFIP-derived scaffolds.

3.4. Bone tissue development

Distribution of bone tissue matrix was evaluated through immunolocalization of bone matrix proteins after 7 weeks of culture in osteogenic medium. The expression of OPN, BSP and collagen type

A

Antigen	CD29	CD105	CD45	CD34	CD44	CD73	CD90	PE Ctrl	FITC Ctrl	PBS Ctrl
Expression%	99.03	98.82	11.87	93.94	12.7	88.48	93.46	8.1	7.4	7.1

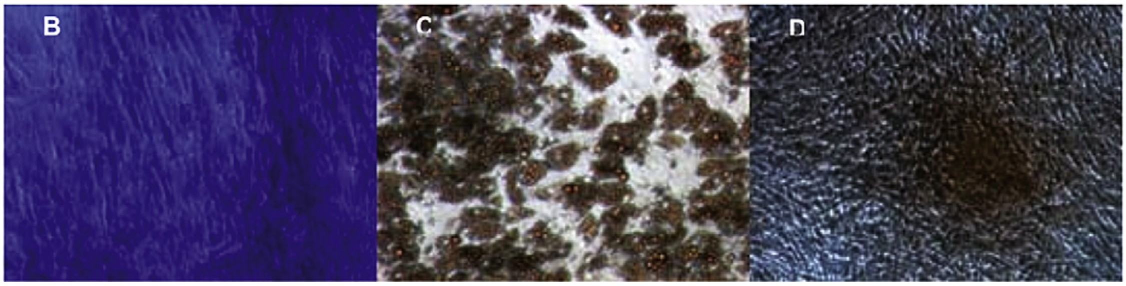

Fig. 2. Phenotypic characterization and evaluation of the multipotency of human adipose stem cells. (A) Percentage of antigen expression in primary hASCs. (B) Toluidine blue staining of undifferentiated stromal cells. (C) Oil Red O staining for adipogenesis. (D) Alizarin Red staining for osteogenesis.

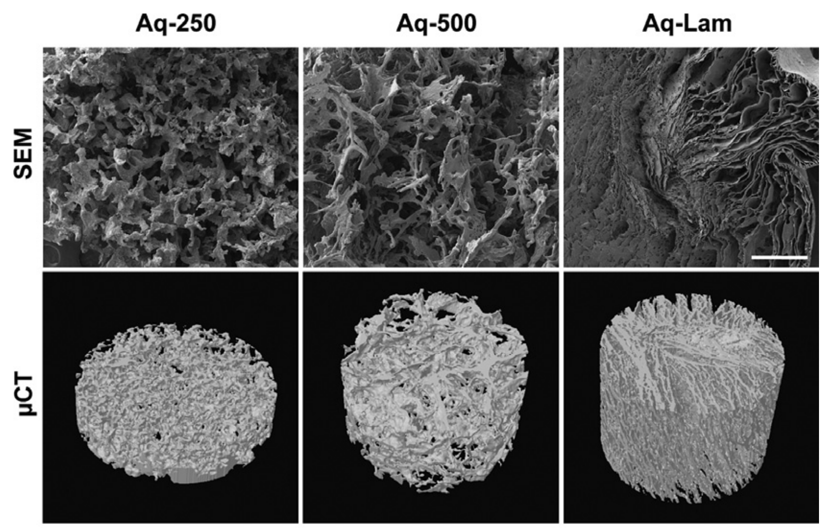

	Aq-250	Aq-500	Aq-Lam
Porosity (%)	75.95 ± 1.55	86.62 ± 0.84	64.25 ± 8.82
Interconnectivity (%)	90.97 ± 3.02	97.83 ± 0.61	63.25 ± 21.13
Average pore size (μm)	139.74 ± 30.05	254.32 ± 13.64	126.24 ± 48.16
Trabeculae thickness (μm)	59.98 ± 5.88	56.51 ± 3.55	63.13 ± 20.47

Fig. 3. Aqueous-based silk fibroin scaffolds characterization. Top row: SEM images of Aq-250, Aq-500 and Aq-Lam scaffolds, demonstrating pore morphology and wall surface. Scale bar = 500 μm. Middle row: μCT 3-D reconstruction of silk fibroin scaffolds. Bottom row: morphometric parameters obtained by μCT analysis.

I (Col I) were similar in both small (Aq-250) and large (Aq-500) pore size aqueous silk sponges (Fig. 5). These bone matrix markers were distributed throughout the decellularized bone scaffold. The most robust groups were the aqueous lamellar and HFIP-derived sponges, with high intensities of immunolocalization of OPN and BSP, and a somewhat lower intensity of Col I. The cells maintained their osteogenic properties throughout the duration of culture.

3.5. Quantification of bone differentiation parameters

To complement the immunostains shown in Fig. 5, quantitative biochemical data were obtained to determine the amounts of bone differentiation markers. AP activity, an early marker of osteoblastic phenotype, peaked after 2 weeks of culture, as expected, at similar levels in all groups, except for significantly higher expression in the Aq-Lam group (Fig. 7A). As an indicator of extracellular matrix (ECM) maturation and calcification, AP activity levels decreased by 7 weeks of culture. The calcium deposition increased in parallel to the decrease in AP activity, between weeks 2 and 7, with significantly higher levels in HFIP and decellularized bone scaffolds than in other groups (Fig. 7B). Consistent with the biochemically measured calcium levels, the BV detected by μCT analysis was also higher in the HFIP than in the aqueous scaffolds, and was highest in the decellularized bone group (Fig 7C). Although not significantly different, HFIP-derived sponges (HFIP-400) demonstrated an increased bone volume relative to the aqueous-based groups. The equilibrium modulus of the constructs was also highest for the decellularized bone group, and higher for the HFIP than the aqueous spherical-porous scaffolds (Fig. 7D). Interestingly, the aqueous-based silk fibroin lamellar

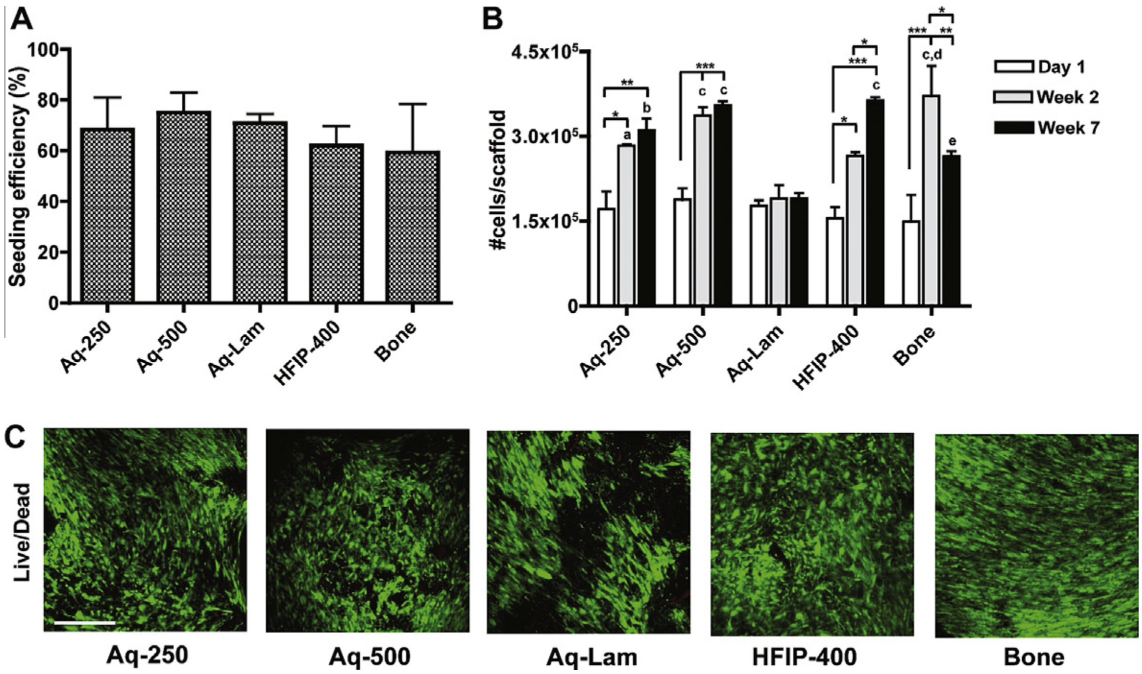

Fig. 4. Cell viability and proliferation. (A) Cell seeding efficiency. No significant differences were observed between groups. (B) Cell proliferation evaluated by changes in the number of cells per scaffold. $^{*}p < 0.05$, $^{**}p < 0.01$, $^{***}p < 0.001$; (a) $p < 0.05$, (b) $p < 0.01$, (c) $p < 0.001$ to Aq-Lam; (d) $p < 0.05$ to Aq-250 and HFIP-400; (e) $p < 0.05$ to Aq-500 and HFIP-400; (C) cell viability (Live/Dead assay) after 7 weeks of culture. Scale bar = 200 μm.

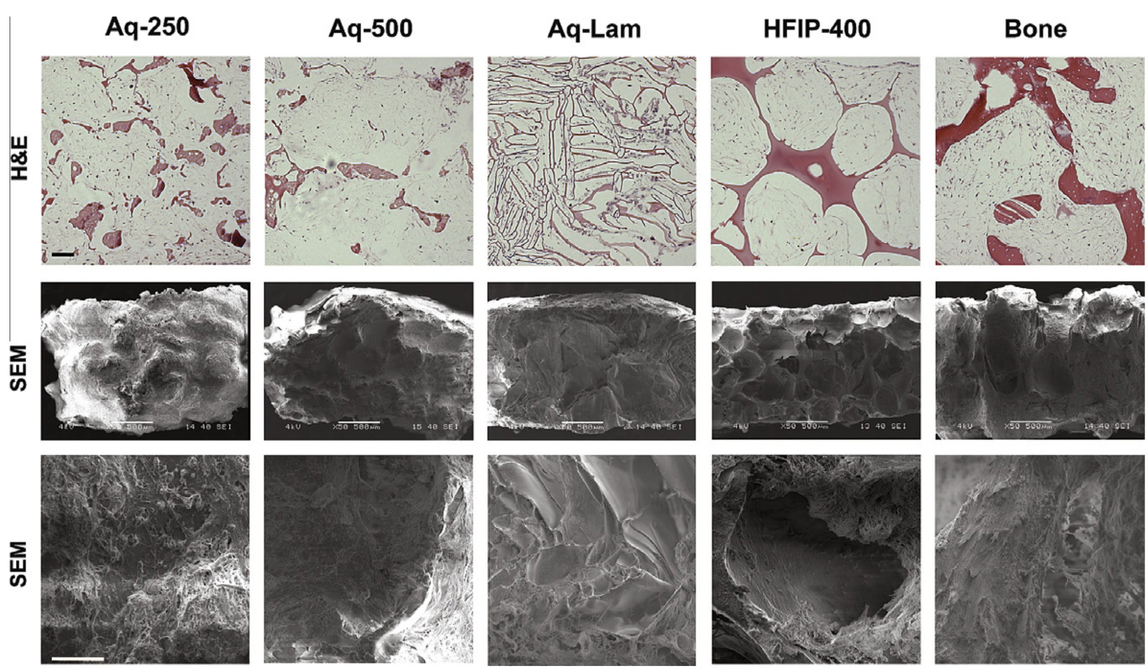

Fig. 5. Scaffold structure. Constructs were analyzed after 7 weeks of culture. Top row: H&E staining, scale bar = 200 μm. Middle row: SEM images, ×50, scale bar = 500 μm. Bottom row: SEM images, ×400, scale bar = 50 μm.

structure (Aq-Lam) was threefold stiffer than the corresponding aqueous-based porous silk sponges (Aq-250 and Aq-500) ($p < 0.01$). This is evidence of the importance of the scaffold architecture for the resulting mechanical properties of the engineered tissue. Furthermore, the mineralized tissue was better distributed in the HFIP-400 group (Fig. 7E), where small sphere-like structures were observed, whereas in the aqueous groups mineral was deposited less uniformly throughout the construct, forming plate-like structures.

4. Discussion

In this study, we investigated different types of silk-based scaffolds by various fabrication methods, as a potential material of choice for bone tissue engineering applications [19,26], with focus on hASCs as a cell source. Notably, the hASCs showed expression patterns of surface markers characteristic for mesenchymal stem cell ($CD105^{+}$, $CD73^{+}$, $CD90^{+}$, $CD45^{-}$, $CD44^{-}$) (Fig. 2A) consistent with that of the BM-MSCs, which have been successfully used for

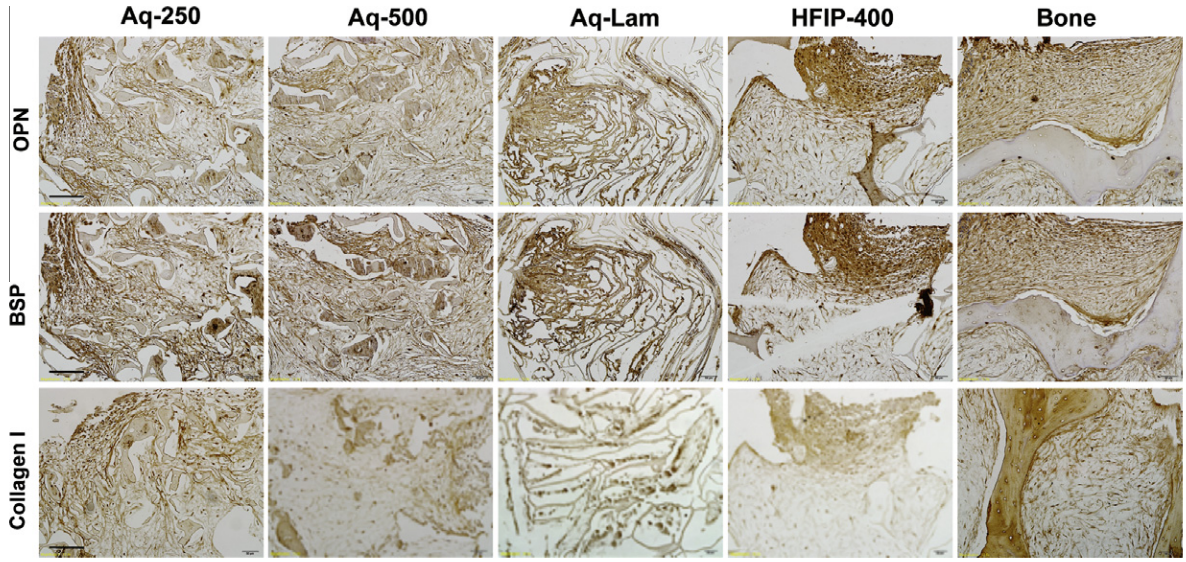

Fig. 6. Accumulation of bone matrix proteins in tissue constructs. Data are shown after 7 weeks of culture. Top row: OPN; middle row: BSP; bottom row: Col I. Scale bar = 100 μm.

engineering of bone [40]. The multi-lineage differentiation capability (adipogenic and osteogenic) was also verified and similar to that observed for BM-MSCs (Fig. 2B–D). Our previous studies confirmed the maintenance of a high level of expression of the surface markers for hASC stemness and differentiation capability over several passages [32].

Four different types of silk scaffolds were investigated. Aqueous-based silk fibroin sponges were produced with three distinct pore sizes and morphologies: the Aq-250 structure had an average porogen size of 375 μm, which has been accepted as the optimal pore size for bone formation [41]; Aq-500 aimed at resembling the pore size of native trabecular bone [42]; and Aq-Lam resembled the lamellar microstructure of bone [26]. In addition to aqueous-based scaffolds, HFIP-400, another silk scaffold, which has previously demonstrated rapid bone formation when cultured with BM-MSCs, was also studied [21]. While the Aq-250, Aq-500 and HFIP-500 groups present a spherical pore formed by salt leaching, the Aq-Lam group presents a structure where the pore walls form parallel lamellae, which are aligned in several directions (Fig. 3). Decellularized trabecular bone was used as a "gold standard". The hASC osteogenic activity and bone formation among the different scaffolds were directly compared.

The differences in the silk scaffolds due to their preparation methods did not affect the hASC seeding efficiency (Fig. 4A), suggesting insignificant effects of solvent used and pore morphology on hASC attachment. After cultivation for 7 weeks, cell numbers increased in all groups except Aq-Lam (Fig. 4B). The data suggest that cells have limited available space to proliferate once porosity, pore size and interconnectivity (Fig. 3, bottom) are significantly inferior to those of aqueous-derived scaffolds with spherical pores (Aq-250 and Aq-500). The seeding efficiency in Aq-Lam group was not inferior to that of the other groups, which may indicate that cells were efficiently seeded in the structure, and might have become saturated, limiting cell proliferation and stimulating cell differentiation. Both Aq-250 and Aq-500 did not demonstrate a significant difference regarding proliferation, which can be explained by contact inhibition [43]. Contrarily, the proliferation data of HFIP-400 show that there was a continuous increase throughout the culture period, but the cell numbers at the end of culture were no higher than in the other spherical-pore silk structures (Aq-250 and Aq-500). It seems that the cells proliferated at a slower rate, which can be explained by the scaffold's smoother pore surfaces, as has been reported elsewhere [3].

Over 7 weeks, hASCs differentiated and expressed osteogenic markers in all groups, albeit with different intensities. Bone tissue development for aqueous-based scaffolds, both small and large pore size (Aq-250 and Aq-500), was found to be similar. Pore size did not influence seeding efficiency or cell proliferation. Cell viability, morphology (Fig. 4C) and distribution throughout individual pores or across the entire scaffold were very similar between the two groups (Fig. 5, top). Bone proteins, such as OPN, BSP and Col I, were produced and retained in the form of extracellular matrix to an analogous extent (Fig. 5). In addition, pore size did not affect the amount of P production, calcium deposition or bone volume. The equilibrium moduli of Aq-250 and Aq-500 were also similar. We postulate that, while smaller pores promote increased the mechanical strength, the larger pores were associated with a more homogeneous matrix [25] – characteristics which may compensate the compressive capacity. Of the four silk scaffold groups in this study, Aq-250 and Aq-500 were inferior.

Lamellar aqueous-based silk fibroin scaffolds (Aq-Lam) showed some interesting features. The equilibrium modulus was the highest among all silk scaffold groups at the beginning of culture, which might be due to the small inter-lamellar distance (25–100 μm), but also demonstrated the most significant increase in mechanical properties after culture ($p < 0.01$) (Fig. 7D). This reflects the significant calcium increase observed in this group ($p < 0.05$) (Fig. 7B), and the increased deposition of bone proteins such as OPN, BSP and Col I (Fig. 6). Furthermore, the cells of the Aq-Lam group expressed the most AP activity at week 2 of culture (Fig. 7A), showing enhancement of osteogenic differentiation. Absolute values of calcium change and bone volume (Fig. 7B and C), though, were similar to those observed for Aq-250 and Aq-500 groups. This result is not surprising, as the native lamellar bone is generated more slowly than woven bone and is less mineralized [44].

Out of the four silk scaffold groups, the HFIP-derived sponge supported the most hASC osteogenic induction and bone-like tissue formation. The similarity of cell proliferation and morphology to aqueous-based scaffolds demonstrated that the higher silk concentration and HFIP solvent did not alter the abilities of hASCs to adhere and proliferate. However, HFIP-derived scaffolds enhanced hASC

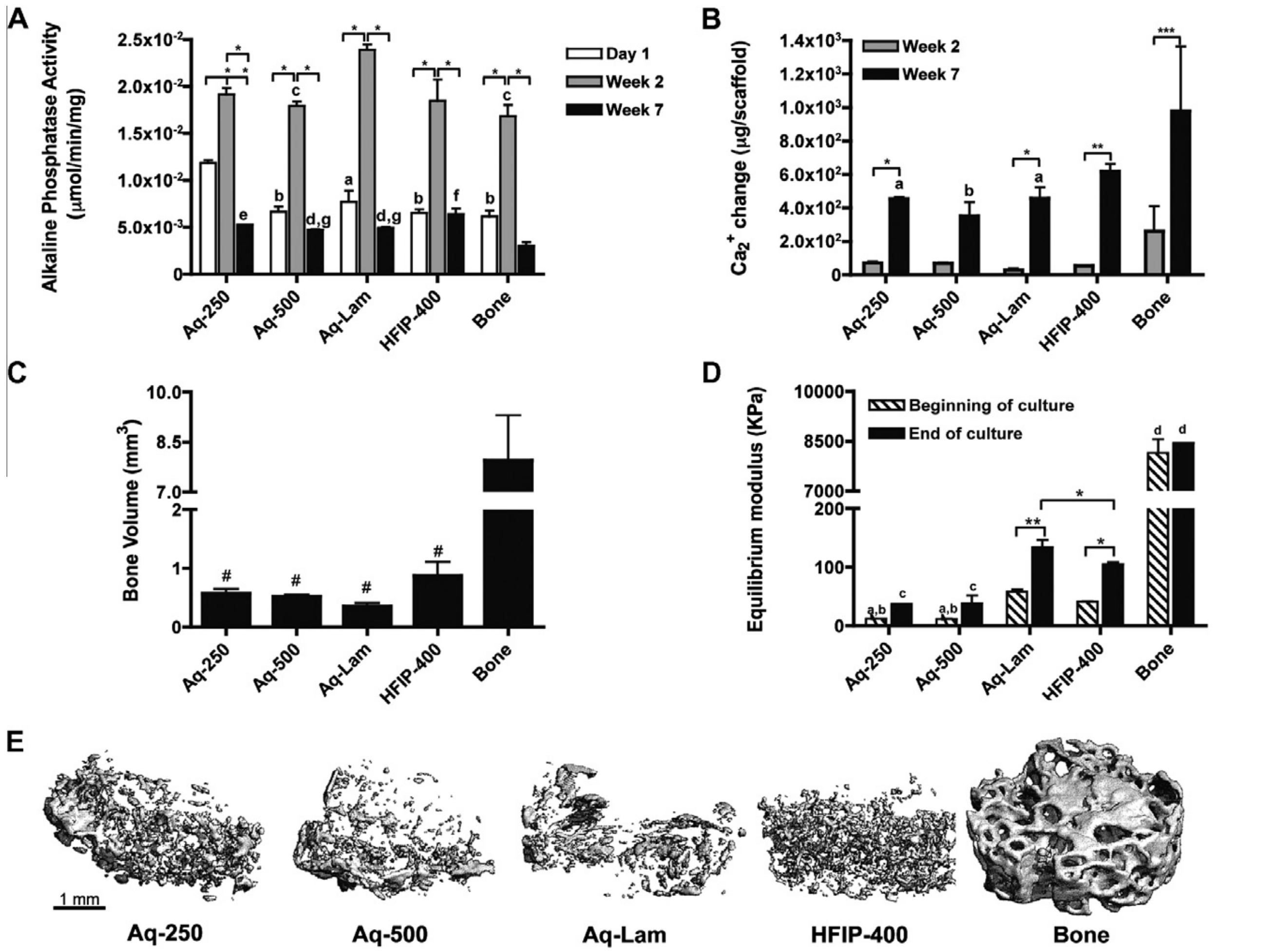

Fig. 7. Biochemical and mechanical characterization of constructs. (A) AP activity: $^{*}p < 0.001$; (a) $p < 0.05$, (b) $p < 0.01$ to Aq-250; (c) $p < 0.05$ to Aq-Lam; (d) $p < 0.05$, (e) $p < 0.01$, (f) $p < 0.001$ to bone; (g) $p < 0.05$ to HFIP-400. (B) Calcium change from day 1 measured at 2 and 7 weeks of culture: $^{*}p < 0.05$, $^{**}p < 0.01$, $^{***}p < 0.001$; (a) $p < 0.05$, (b) $p < 0.01$ to bone. (C) BV of constructs at week 7: $^{\#}p < 0.05$ to bone. (D) Equilibrium modulus at the beginning and end of culture: $^{*}p < 0.05$, $^{**}p < 0.01$; (a) $p < 0.05$ to HFIP-400, (b) $p < 0.001$ to Aq-Lam, (c) $p < 0.001$ to HFIP-400 and Aq-Lam, (d) $p < 0.001$ to all other groups. (E) μCT Reconstruction images of constructs after 5 weeks of culture. Scale bar = 1 mm.

deposition of matrix proteins (OPN, BSP, Col I) (Fig. 6) and mineralization, quantified by calcium retention in the scaffold (Fig. 7B) and mineralized BV (Fig. 7C). According to μCT reconstruction of cultured constructs (Fig. 7E), mineral was evenly distributed throughout the scaffold in this group, showing homogeneous osteogenic activity of hASCs. Regarding mechanical properties, although the equilibrium modulus of HFIP-based silk scaffold was higher than aqueous-based constructs with spherical pores even from the beginning of culture, possibly due to the higher concentration of silk material (Fig. 7D), among these three groups, HFIP-400 was the only group demonstrating a significant increase in mechanical properties from the beginning to the end of culture ($p < 0.05$). This can be justified by the deposition of a more robust ECM, composed of both ECM proteins and calcification, as discussed above.

Decellularized trabecular bone scaffolds have been used successfully in bone tissue engineering studies [32,33,45]. Although the bone-forming structure and mechanical properties of the silk scaffolds were inferior to the trabecular bone scaffold, the osteogenic cellular activities in the Aq-250 and Aq-500 groups were similar to the bone scaffold and were enhanced in the Aq-Lam and HFIP-400 groups (Figs. 6 and 7A).

Taken together, the data collected in this study are consistent with the conceptual model shown in Fig. 8. Two distinguishable scaffold properties – scaffold architecture and mechanical stiffness – appear to affect bone formation (Fig. 8). First, scaffold stiffness is positively correlated with osteogenic differentiation of hASCs, resulting in an increase in bone ECM secretion (Fig. 8A). The importance of mechanical properties in bone tissue engineering has been well established [19,46]. Similar to previous findings, HFIP-derived silk fibroin scaffolds, which exhibited higher stiffness as compared to aqueous-based silk fibroin scaffolds, appear to provided a better platform for bone formation. Second, the scaffold structure appears to alter cellular activities as well as bone tissue formation. A porous lamellar morphology is postulated to benefit hASC osteogenic differentiation into lamellar bone, which contains fewer cells but has higher mechanical properties once it is highly organized, while a spherical porous structure leads to the development of woven bone, which contains higher cellularity and mineral density but is far less organized (Fig. 8B) [44,47].

Based on the extensive work already reported on bone tissue engineering with BM-MSC on silk scaffolds and the data we present in this study, we speculate that hASC are a good alternative cell source to BM-MSC for bone TE. For instance, our research group has reported the outcomes of engineered bone grafts by culturing BM-MSC in similar HFIP scaffolds up to 5 and 10 weeks [6], and, even when culturing in dynamic conditions by flow perfusion, bone-related outcomes were less patent than those obtained in the present study.

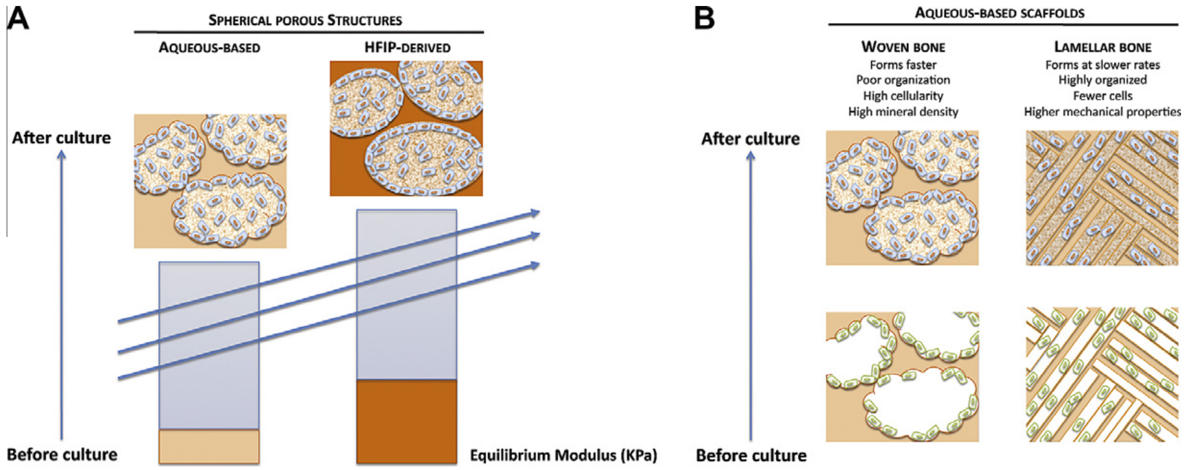

Fig. 8. Proposed mechanism of regulation of bone formation by scaffold architecture and stiffness. (A) Scaffold mechanics. Mechanically stronger HFIP-derived silk scaffolds promote osteogenic differentiation of hASCs to result in increased BV, calcium content and bone protein deposition, as compared to aqueous-based scaffolds. (B) Scaffold architecture. A sponge-like architecture with spherical pores serves as a template for the formation of woven bone, while a lamellar porous architecture serves as a template for the formation of lamellar bone.

5. Conclusions

This study has demonstrated the optimization potential of silk scaffolds in terms of structure (porosity, pore dimensions and pore geometry) and biomechanics for bone tissue engineering applications. We have demonstrated that human adipose-derived stem cells interpret the extracellular environment, by responding differently to the architecture of silk scaffolds and producing bone-like extracellular matrix in a manner that appears to depend on the structure and stiffness of the scaffolds. Based on the collected data, we have proposed a conceptual model that correlates bone tissue formation with the architecture and stiffness of silk scaffolds, which emphasizes the importance of appropriate scaffold design when engineering bone.

Acknowledgements

We gratefully acknowledge Rita Duarte for her help with experiments, and the support of this work by funding from the NIH (DE161525 andEB02520 to G.V.N.) and an FCT Ph.D Grant (SFRH/BD/42316/2007 to C.C.).

Appendix A. Figures with essential colour discrimination

Certain figures in this article, particularly Figs. 2–7 and 8, are difficult to interpret in black and white. The full colour images can be found in the on-line version, at http://dx.doi.org/10.1016/j.actbio.2012.03.019.

References

[1] Puppi D, Chiellini F, Piras AM, Chiellini E. Polymeric materials for bone and cartilage repair. Prog Polym Sci 2010;35:403–40.
[2] Salgado AJ, Coutinho OP, Reis RL. Bone tissue engineering: state of the art and future trends. Macromol Biosci 2004;4:743–65.
[3] Kim HJ, Kim HS, Matsumoto A, Chin IJ, Jin HJ, Kaplan DL. Processing windows for forming silk fibroin biomaterials into a 3D porous matrix. Aust J Chem 2005;58:716–20.
[4] Horan RL, Antle K, Collette AL, Huang YZ, Huang J, Moreau JE, et al. In vitro degradation of silk fibroin. Biomaterials 2005;26:3385–93.
[5] Saitow C, Kaplan DL, Castellot JJ. Heparin stimulates elastogenesis: application to silk-based vascular grafts. Matrix Biol 2011;30:346–55.
[6] Bhumiratana S, Grayson WL, Castaneda A, Rockwood DN, Gil ES, Kaplan DL, et al. Nucleation and growth of mineralized bone matrix on silk–hydroxyapatite composite scaffolds. Biomaterials 2011;32:2812–20.
[7] Chao PHG, Yodmuang S, Wang XQ, Sun L, Kaplan DL, Vunjak-Novakovic G. Silk hydrogel for cartilage tissue engineering. J Biomed Mater Res B 2010;95B:84–90.
[8] Yan LP, Oliveira JM, Oliveira AL, Caridade SG, Mano JF, Reis RL. Macro/micro porous silk fibroin scaffolds with potential for articular cartilage and meniscus tissue engineering applications. Acta Biomater 2012;8:289–301.
[9] Wang YZ, Kim HJ, Vunjak-Novakovic G, Kaplan DL. Stem cell-based tissue engineering with silk biomaterials. Biomaterials 2006;27:6064–82.
[10] Murphy AR, Kaplan DL. Biomedical applications of chemically-modified silk fibroin. J Material Chem 2009;19:6443–50.
[11] Hofmann S, Knecht S, Langer R, Kaplan DL, Vunjak-Novakovic G, Merkle HP, et al. Cartilage-like tissue engineering using silk scaffolds and mesenchymal stem cells. Tissue Eng 2006;12:2729–38.
[12] Wang YZ, Kim UJ, Blasioli DJ, Kim HJ, Kaplan DL. In vitro cartilage tissue engineering with 3D porous aqueous-derived silk scaffolds and mesenchymal stem cells. Biomaterials 2005;26:7082–94.
[13] Wang YZ, Blasioli DJ, Kim HJ, Kim HS, Kaplan DL. Cartilage tissue engineering with silk scaffolds and human articular chondrocytes. Biomaterials 2006;27:4434–42.
[14] Mauney JR, Nguyen T, Gillen K, Kirker-Head C, Gimble JM, Kaplan DL. Engineering adipose-like tissue in vitro and in vivo utilizing human bone marrow and adipose-derived mesenchymal stem cells with silk fibroin 3D scaffolds. Biomaterials 2007;28:5280–90.
[15] Kang JH, Gimble JM, Kaplan DL. In vitro 3D model for human vascularized adipose tissue. Tissue Eng A 2009;15:2227–36.
[16] Lovett M, Eng G, Kluge JA, Cannizzaro C, Vunjak-Novakovic G, Kaplan DL. Tubular silk scaffolds for small diameter vascular grafts. Organogenesis 2010;6:217–24.
[17] Altman GH, Horan RL, Lu HH, Moreau J, Martin I, Richmond JC, et al. Silk matrix for tissue engineered anterior cruciate ligaments. Biomaterials 2002;23:4131–41.
[18] Chen JS, Altman GH, Karageorgiou V, Horan R, Collette A, Volloch V, et al. Human bone marrow stromal cell and ligament fibroblast responses on RGD-modified silk fibers. J Biomed Material Res A 2003;67A:559–70.
[19] Kim HJ, Kim UJ, Vunjak-Novakovic G, Min BH, Kaplan DL. Influence of macroporous protein scaffolds on bone tissue engineering from bone marrow stem cells. Biomaterials 2005;26:4442–52.
[20] Meinel L, Karageorgiou V, Hofmann S, Fajardo R, Snyder B, Li CM, et al. Engineering bone-like tissue in vitro using human bone marrow stem cells and silk scaffolds. J Biomed Material Res A 2004;71A:25–34.
[21] Marolt D, Augst A, Freed LE, Vepari C, Fajardo R, Patel N, et al. Bone and cartilage tissue constructs grown using human bone marrow stromal cells, silk scaffolds and rotating bioreactors. Biomaterials 2006;27:6138–49.
[22] Vepari C, Kaplan DL. Silk as a biomaterial. Prog Polym Sci 2007;32:991–1007.
[23] Nazarov R, Jin HJ, Kaplan DL. Porous 3-D scaffolds from regenerated silk fibroin. Biomacromolecules 2004;5:718–26.
[24] Kim UJ, Park JY, Li CM, Jin HJ, Valluzzi R, Kaplan DL. Structure and properties of silk hydrogels. Biomacromolecules 2004;5:786–92.
[25] Kim UJ, Park J, Kim HJ, Wada M, Kaplan DL. Three-dimensional aqueous-derived biomaterial scaffolds from silk fibroin. Biomaterials 2005;26:2775–85.
[26] Oliveira AL, Sun L, Kim HJ, Hu X, Rice W, Kluge J, et al. Designing silk-based 3-D architectures with controlled lamellar morphology. Tissue Eng A 2008;14:718–9.
[27] Park SH, Gil ES, Shi H, Kim HJ, Lee K, Kaplan DL. Relationships between degradability of silk scaffolds and osteogenesis. Biomaterials 2010;31:6162–72.

[28] Rockwood DN, Gil ES, Park SH, Kluge JA, Grayson W, Bhumiratana S, et al. Ingrowth of human mesenchymal stem cells into porous silk particle reinforced silk composite scaffolds: an in vitro study. Acta Biomaterial 2011;7:144–51.
[29] Gimble JM, Guilak F, Bunnell BA. Clinical and preclinical translation of cell-based therapies using adipose tissue-derived cells. Stem Cell Res Ther 2010;1:19.
[30] Zuk PA, Zhu M, Mizuno H, Huang J, Futrell JW, Katz AJ, et al. Multilineage cells from human adipose tissue: implications for cell-based therapies. Tissue Eng 2001;7:211–28.
[31] Schaffler A, Buchler C. Concise review: adipose tissue-derived stromal cells – basic and clinical implications for novel cell-based therapies. Stem cells (Dayton, Ohio) 2007;25:818–27.
[32] Frohlich M, Grayson WL, Marolt D, Gimble JM, Kregar-Velikonja N, Vunjak-Novakovic G. Bone grafts engineered from human adipose-derived stem cells in perfusion bioreactor culture. Tissue Eng A 2010;16:179–89.
[33] Grayson WL, Bhumiratana S, Cannizzaro C, Chao PH, Lennon DP, Caplan AI, et al. Effects of initial seeding density and fluid perfusion rate on formation of tissue-engineered bone. Tissue Eng A 2008;14:1809–20.
[34] McIntosh K, Zvonic S, Garrett S, Mitchell JB, Floyd ZE, Hammill L, et al. The immunogenicity of human adipose-derived cells: temporal changes in vitro. Stem Cells 2006;24:1246–53.
[35] Mitchell JB, McIntosh K, Zvonic S, Garretta S, Floyd ZE, Kloster A, et al. Immunophenotype of human adipose-derived cells: temporal changes in stromal-associated and stem cell-associated markers. Stem Cells 2006;24:376–85.
[36] Yu G, Wu X, Dietrich MA, Polk P, Scott LK, Ptitsyn AA, et al. Yield and characterization of subcutaneous human adipose-derived stem cells by flow cytometric and adipogenic mRNA analyzes. Cytotherapy 2010;12:538–46.
[37] Liu XWS, Sajda P, Saha PK, Wehrli FW, Guo XE. Quantification of the roles of trabecular microarchitecture and trabecular type in determining the elastic modulus of human trabecular bone. J Bone Mineral Res 2006;21:1608–17.
[38] Mauck RL, Soltz MA, Wang CCB, Wong DD, Chao PHG, Valhmu WB, et al. Functional tissue engineering of articular cartilage through dynamic loading of chondrocyte-seeded agarose gels. J Biomech Eng-T Asme 2000;122:252–60.
[39] Gimble JM, Katz AJ, Bunnell BA. Adipose-derived stem cells for regenerative medicine. Circulat Res 2007;100:1249–60.
[40] Gimble JM, Bunnell BA, Chiu ES, Guilak F. Concise review: adipose-derived stromal vascular fraction cells and stem cells: let's not get lost in translation. Stem cells (Dayton, Ohio) 2011;29:749–54.
[41] Karageorgiou V, Tomkins M, Fajardo R, Meinel L, Snyder B, Wade K, et al. Porous silk fibroin 3-D scaffolds for delivery of bone morphogenetic protein-2 in vitro and in vivo. J Biomed Material Res A 2006;78A:324–34.
[42] Keaveny TM, Morgan EF, Niebur GL, Yeh OC. Biomechanics of trabecular bone. Annu Rev Biomed Eng 2001;3:307–33.
[43] Huang S, Ingber DE. From stem cells to functional tissue architecture. In: Sell S, editor. Stem cells handbook. Totowa, NJ: Humana Press Inc.; 2004.
[44] McKenzie JA, Silva MJ. Comparing histological, vascular and molecular responses associated with woven and lamellar bone formation induced by mechanical loading in the rat ulna. Bone 2011;48:250–8.
[45] Grayson WL, Frohlich M, Yeager K, Bhumiratana S, Chan ME, Cannizzaro C, et al. Regenerative medicine special feature: engineering anatomically shaped human bone grafts. Proc Natl Acad Sci USA 2009.
[46] Thomson RC, Shung AK, Yaszemski MJ, Mikos AG. Polymer scaffold processing. In: Lanza RP, Langer R, Vacanti J, editors. Principles of tissue engineering. San Diego: Academic Press; 2000. p. 251–62.
[47] Martin RB, Burr DB, Sharkey NA. Skeletal tissue mechanics. New York: Springer-Verlag Inc.; 1998.